



Metal dusting as a key route to produce functionalized carbon nanofibers

Arina R. Potylitsyna^{1,2} · Ilya V. Mishakov¹ · Yury I. Bauman¹ · Lidia S. Kibis¹ · Yury V. Shubin³ · Mikhail N. Volochaev⁴ · Maxim S. Melgunov¹ · Aleksey A. Vedyagin¹

Received: 6 December 2021 / Accepted: 16 January 2022 / Published online: 30 January 2022
© Akadémiai Kiadó, Budapest, Hungary 2022

Abstract

The present paper reports a new method of producing N-doped carbon nanofibers via metal dusting of a ternary NiMoW alloy in the atmosphere containing C_2HCl_3 and CH_3CN vapors at 600 °C. The initial alloy was prepared by a co-precipitation technique. The carbon deposition was monitored gravimetrically. The early stages of the metal dusting process were studied in detail using scanning and transmission electron microscopies. It was established that the rapid disintegration of the microdispersed NiMoW alloy with the formation of nanosized particles catalyzing the growth of carbon filaments occurs within the first 5 min of the reaction. The presence of C_2HCl_3 vapors in the reaction medium was shown to be the urgent condition to provide efficient metal dusting. The effect of the CH_3CN concentration in the trichloroethylene-containing reaction mixture on the carbon deposition is investigated. As observed, the CH_3CN content noticeable affects the carbon yield (after 2 h of reaction). The dome-shaped dependence of carbon yield reaches its maximal value of ~200 g/g(cat) at a CH_3CN concentration of 33 vol%. According to X-ray photoelectron spectroscopy, the obtained carbon filaments are functionalized with Cl (0.1–1.2 wt%), O (3–6 wt%), and N (0.5–1.3 wt%). The prepared carbon filaments possess a segmented secondary structure, which is typical for carbon nanomaterials derived via catalytic decomposition of chlorine-substituted hydrocarbons. Low-temperature nitrogen adsorption measurement revealed that the specific surface area of the N-containing samples varies in a range from 370 to 550 m²/g.

✉ Aleksey A. Vedyagin
vedyagin@catalysis.ru

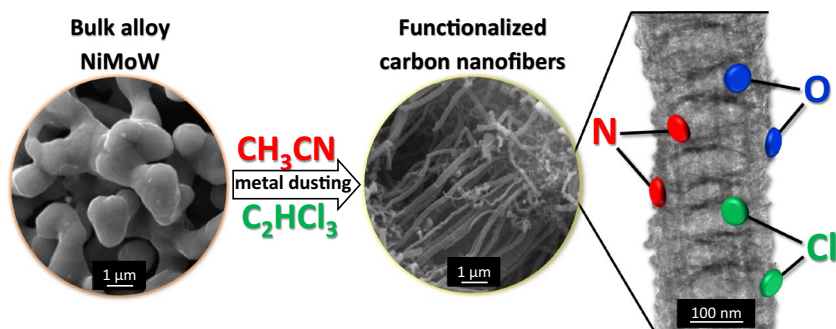
¹ Borekov Institute of Catalysis, pr. Ac. Lavrentieva, 5, Novosibirsk, Russia 630090

² Novosibirsk State University, str. Pirogova 2, Novosibirsk, Russia 630090

³ Nikolaev Institute of Inorganic Chemistry, Ac. Lavrentieva 3, Novosibirsk, Russia 630090

⁴ Kirensky Institute of Physics, Akademgorodok, 50/38, Krasnoyarsk, Russia 660036

Graphical abstract



Keywords Metal dusting · Ternary nickel–molybdenum–tungsten alloy · Trichloroethylene · Acetonitrile · Functionalized carbon nanofibers

Introduction

Metal dusting (MD) or carbon erosion is a phenomenon of complete destruction of metal items based on Fe, Co, and Ni at elevated temperature (400–800 °C) in a carbon-containing medium, which is accompanied by the formation of dispersed metal particles and graphite phase [1, 2]. This irreversible process actually causes the destruction of chemical reactors operating under such conditions. On the other hand, even this “undesirable” phenomenon currently attracts significant attention from researchers since it can be considered beneficial [3, 4]. The dispersed particles, formed because of spontaneous disintegration of the initial metal or alloy, act as centers for the carbon nanostructures’ growth. Therefore, the MD process can be purposefully applied to obtain carbon nanofibers (CNFs) or other carbon-containing nanomaterials, including metal–carbon composites, thus serving as a promising tool for their controllable synthesis [5–11].

Among the wide variety of carbon materials, CNFs attract the greatest attention due to the unique combination of physicochemical properties (strength, developed specific surface area, chemical inertness, and good electrical and thermal conductivity) and relatively low cost. These materials have already found their application as catalyst carriers [12, 13], sorbents of toxic wastes [14, 15], products for electronics [16, 17], drug delivery agents [18], and reinforcing additives in constructive composites [19–23].

The heteroatom-functionalized CNFs (N, Cl, O, B, P, etc.) are even of greater interest since the introduction of additional atoms into the structure of carbon filaments significantly affects the reactivity and electrical conductivity of the resulting material [24], which, in turn, expands the area of their application. Doping of carbon fibers with nitrogen (N-CNF) is especially often mentioned in the literature. It is well known that nitrogen atoms on the surface of carbon nanomaterials are capable

of stabilizing carbon-supported catalysts by increasing the dispersion of metal particles [25]. On the other hand, in composite science, the presence of N-functional groups increases the adhesion between the carbon filler and the modifying polymer matrix [26]. Nitrogen-doped carbon nanomaterials are already used in practice for the storage and transformation of energy in fuel cells [27], as electrochemical sensors [28], adsorbents, and supports for catalysts in such processes as selective hydrogenation of acetylene and hydrodechlorination of chlorinated aromatic compounds [29, 30].

N-doped CNFs can be obtained via ‘one-pot’ synthesis by joint decomposition of carbon- and nitrogen-containing substrates (for example, C_2H_4 and NH_3) [31] or via post-functionalization of preliminary prepared CNFs using an N-containing modifying agent (for example, pyridine) [29]. The third approach, which was proposed recently, is based on the joint catalytic pyrolysis of C- and N-containing reagents over self-organizing catalysts [32]. The formation of the active catalytic particles from bulk nickel-based alloy occurs under the action of the reaction medium via the MD route. This approach seems to be the least time-consuming since it allows combining the stages of the catalyst preparation and N-CNFs synthesis.

At the same time, the presence of chlorine in the reaction system affects the growth mechanism of carbon nanofibers, largely determining their unique structure [33]. The process of the bulk alloys’ disintegration in an aggressive atmosphere, simultaneously containing chlorine and hydrogen, is accelerated due to chlorination/dechlorination reactions occurring on the metal surface. These reactions also provide a pulse mode of the fiber growth resulting in the appearance of the segmented structure [34]. It should be emphasized that many chlorine-substituted hydrocarbons ($C_2H_4Cl_2$, C_2HCl_3) are the main components of toxic industrial waste that harm the environment [35]. The proposed approach, based on the application of MD for the CNFs synthesis, gives a possibility to develop a new method for processing such compounds into valuable carbon nanomaterials.

Among the metals of the iron subgroup (Fe, Co, and Ni), which are active in the process under consideration, nickel catalysts are most commonly used to catalyze organochlorine compounds’ pyrolysis since they demonstrate the highest resistance to deactivation [36]. In addition, the introduction of promoting additives (Mo, W, Pd, etc.) into the alloy composition significantly increases the stability and improves the performance of the Ni-based catalysts [37–39]. As was previously established, Mo is one of the most promising promoters. Its addition allows increasing the carbon yield in the catalytic decomposition of 1,2-dichloroethane by almost two times if compared with pure Ni [40]. In the case of ternary NiMoW alloy, the activity grows even more impressively [39].

In the present work, the possibility of using the MD process for the synthesis of heteroatom-functionalized CNFs is demonstrated. Trichloroethylene (TCE) and acetonitrile (AN) are chosen as carbon and nitrogen sources, respectively. The presence of chlorine in the C_2HCl_3 molecule makes it possible to significantly accelerate the MD process of the ternary nickel alloy containing 4 wt% Mo and 4 wt% W. The initial stages of the MD process occurring during the joint decomposition of TCE and AN have been investigated. The obtained N-CNFs were characterized by X-ray photoelectron spectroscopy and scanning and transmission

electron microscopies. The effect of the AN concentration on the carbon yield and CNFs characteristics has been revealed as well.

Experimental

Synthesis of the microdispersed NiMoW alloy

Ternary NiMoW alloy containing 92 wt% Ni, 4 wt% Mo, and 4 wt% W was prepared by co-precipitation technique from precursor salts $[\text{Ni}(\text{NH}_3)_6]\text{Cl}_2$ (chemically pure, synthesized in accordance with a published procedure [41]), H_2WO_4 (pure, Vekton, Russia), and $(\text{NH}_4)_6\text{Mo}_7\text{O}_{24}\cdot 4\text{H}_2\text{O}$ (chemically pure, Reachem, Russia), followed by a reduction in a hydrogen atmosphere. Acetone (high purity grade, Vekton, Russia) was used as a precipitating agent. All the reagents were chemically pure and were used without prior purification.

Initially, $(\text{NH}_4)_6\text{Mo}_7\text{O}_{24}\cdot 4\text{H}_2\text{O}$ (0.073 g) and H_2WO_4 (0.054 g) were dissolved in a 50 mL concentrated (25 wt%) aqueous solution of ammonia (high purity grade, Reachem, Russia) at heating. The resulting solution was evaporated to a volume of 30 mL. Then, 3.633 g of $[\text{Ni}(\text{NH}_3)_6]\text{Cl}_2$ was added to the solution with continuous stirring by magnetic stirrer (200 rpm) until complete dissolution. Precipitation was carried out by mixing the resulting solution with a 15-fold volume of acetone (450 mL) cooled to 0 °C. The precipitate was filtered, dried at room temperature for 5 h, and calcined at 800 °C for 1 h under a hydrogen atmosphere. Monometallic Ni used as a reference sample was synthesized similarly.

Characterization of the NiMoW alloy

X-ray diffraction (XRD) analysis of the NiMoW alloy sample was carried out on a Shimadzu XRD-7000 diffractometer (Cu K_α radiation, Ni-filter on a reflected beam) at room temperature. For the analysis of phase composition, the pattern was recorded in a 2θ range of 5° – 107° with a step of 0.1° . The lattice parameter was precisely determined by analyzing the region in a 2θ range of 140° – 148° with a step of 0.02° . Reference diffraction data were taken from the JCPDS database (Ni—PDF card #4-850; Mo—PDF card #42-1120; W—PDF card #4-806). The crystal cell parameters of the solid solution were refined by the Rietveld full-profile analysis of (331) reflection using the PowderCell 2.4 software [42]. Polycrystalline silicon ($a=5.4309 \text{ \AA}$) was used as an external standard. The average crystallite size was estimated by an integral expansion of reflections (111), (200), and (220) using the WinFit 1.2.1 software [43] and Scherrer's formula [44].

The secondary structure of the microdispersed NiMoW alloy was studied by scanning electron microscopy (SEM) on a JSM-6460 microscope (JEOL, Japan) at magnifications from $\times 8$ to $\times 300.000$.

Synthesis of CNFs

The synthesized sample of the microdispersed NiMoW alloy was used as a precursor of a self-organizing catalyst for the synthesis of N-CNFs. The carbon accumulation during the co-decomposition of trichloroethylene and acetonitrile was studied in a flow gravimetric reactor equipped with a McBain balance, which allows measuring the weight of the sample in a real-time regime [45]. The specimen of the initial alloy was 2.0 ± 0.05 mg for all the experiments. The alloy sample was placed in a quartz basket inside the reactor and heated up to 600 °C in an argon flow (11 L/h). Then, the reactor was fed with hydrogen for 10 min to eliminate oxygen from the surface of the alloy. The reduced sample was brought into contact with a reaction mixture simultaneously containing argon, hydrogen, and organic substrate vapors (trichloroethylene and/or acetonitrile) at the same temperature. Since both the substrates are liquids, the required concentration of their vapors was achieved by passing the reaction gas through the saturators filled with trichloroethylene and/or acetonitrile. The TCE concentration in the reaction mixture was 8 vol% in all the experiments, while the AN concentration was varied from 25 to 39 vol% by changing the temperature of the corresponding saturator. For most of the experiments, the duration was 2 h. In order to study the MD process at early stages in detail, the experiments were stopped after 2 and 5 min. The cooling of the reactor to room temperature was performed in an argon flow. The deposited carbon product was weighed to calculate the carbon yield value in grams of CNFs per 1 g of catalyst, g/g(cat). Note that the accuracies of the carbon yield values and the carbon deposition rates were $\pm 10\%$ and $\pm 5\%$, respectively. The obtained samples were labeled as TCE/AN(X)_CNF, where X is AN concentration. Correspondingly, the reference samples prepared via decomposition of TCE or AN only were named as TCE/AN(0)_CNF and AN(27)_CNF.

Characterization of CNFs

The structure and morphology of the prepared CNFs were studied by SEM on a JSM-6460 instrument (JEOL, Japan) at magnifications from $\times 8$ to $\times 300,000$. The transmission electron microscopy (TEM) studies were carried out using a Hitachi HT7700 TEM (acceleration voltage 100 kV, W source) equipped with a STEM system and a Bruker Nano XFlash 6T/60 energy dispersive X-ray (EDX) spectrometer.

X-ray photoelectron spectroscopy (XPS) was used to analyze the surface composition and concentration of the functional groups. XPS spectra were recorded on a photoelectron spectrometer ES300 (KRATOS Analytical, UK) using Al K_{α} source (1486.6 eV). The core-level spectra of copper (Cu $2p_{3/2}$) and gold (Au $4f_{7/2}$) foils were used for calibration of the spectrometer. The survey spectra were collected within a range of 0–1100 eV with a step of 1 eV to explore. The core-level spectra of carbon (C 1s), nitrogen (N 1s), and chlorine (Cl 2p) were recorded with a step of 0.1 eV to analyze the charging states of the elements. The estimation of the composition was performed with consideration of the atomic sensitivity factors [46].

The textural characteristics of the CNF samples were studied by the nitrogen adsorption method. N_2 adsorption at 77 K was measured by means of an Autosorb-iQ (Quantachrome, USA) instrument equipped with the oil-free turbomolecular pump—membrane pump system in a range of partial pressure of $10^{-6} < p/p^\circ < 0.99$. Samples were degassed in an oil-free vacuum at 300 °C overnight before the analysis. The typical specimen of the CNFs for analysis was 0.05 g.

Results and discussions

Characterization of the as-prepared NiMoW alloys

As it was recently reported [47], pure nickel undergoes deactivation after a few hours of carbon deposition. The addition of molybdenum and tungsten, individually or jointly, allows improving the catalytic behavior by increasing the activity and stability of the catalyst [39, 40, 48]. Therefore, a previously optimized composition of the ternary NiMoW alloy is considered in the present research. The initial NiMoW alloy was synthesized by high-temperature reductive thermolysis. This method allows obtaining microdispersed materials of a developed porous structure. Thus, the values of specific surface area (SSA) for such materials can reach 10 m²/g. Characterization of the as-prepared alloy by SEM evidenced the so-called ‘sponge-like’ structure of the sample. Fig. S1 (Supplementary Information) shows the typical SEM images of the microdispersed NiMoW alloy. As seen, a uniform porous matrix is composed of fused particles of approximately 2–3 microns in size (Fig. S1a). In the magnified image (Fig. S1b), the interblock boundaries are well seen. Such a porous structure along with developed SSA facilitates a larger area of contact with the reagents and, therefore, enhanced reactivity.

The phase composition of the as-prepared sample was studied by XRD analysis. The recorded pattern is shown in Fig. 1. XRD data for the reference sample of

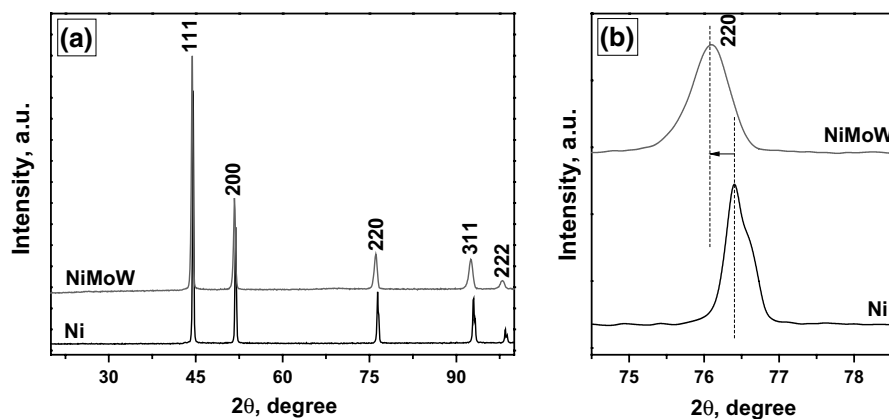


Fig. 1 XRD data for the as-prepared NiMoW sample and pure nickel (reference sample) in 2θ ranges of 20° – 100° (a) and 75° – 77° (b)

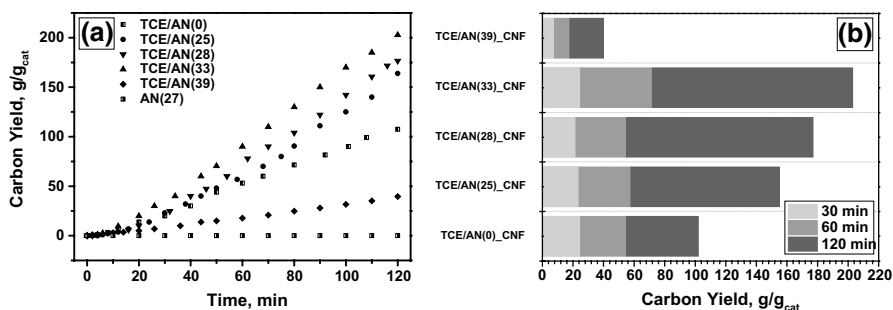


Fig. 2 Time dependence of the carbon yield over the NiMoW alloy during the decomposition of TCE and/or AN at 600 °C (a) and comparison of the carbon yield values obtained after 30, 60, and 120 min of reaction (b)

Table 1 The IP-500 duration and the carbon yield values depending on the composition of the reaction mixture (NiMoW alloy, 2 h, 600 °C)

CNF sample	Composition of the reaction mixture	AN concentration, vol%	IP-500, min	Carbon yield, g/g(cat)
TCE/AN(0)_CNF	TCE/Ar/H ₂	0	10	102
TCE/AN(25)_CNF	TCE + AN/Ar/H ₂	25	12	155
TCE/AN(28)_CNF	TCE + AN/Ar/H ₂	28	12	177
TCE/AN(33)_CNF	TCE + AN/Ar/H ₂	33	14	203
TCE/AN(39)_CNF	TCE + AN/Ar/H ₂	39	20	40
AN(27)_CNF	AN/Ar/H ₂	27	–	0.7

pure nickel is also presented. In both cases, the patterns are represented by a set of reflections, which are characteristic of metallic nickel with a face-centered cubic (FCC) lattice (Fig. 1a). No peaks related to Mo or W are seen. On the other hand, a characteristic shift of nickel reflections to the small angles side should be mentioned (Fig. 1b). From these data, it can be concluded that both the promoting metals, Mo and W, are embedded inside the crystal lattice of nickel, forming a solid solution. The alloying of nickel with tungsten and molybdenum leads to an increase in the FCC lattice parameter of nickel from 3.524 to 3.539 Å. Thus, the synthesized NiMoW sample is a single-phase solid solution based on the FCC lattice of nickel.

Study of the carbon deposition over NiMoW alloy

Fig. 2a shows the time dependence for the carbon accumulation during the catalytic co-decomposition of TCE and AN over the NiMoW sample at 600 °C. According to the recently reported data [49–51], this temperature is optimal for the efficient realization of the metal dusting process over the nickel alloys. Since the current research focuses on the decomposition effect of the multicomponent reaction

mixture containing AN, the concentration of AN vapors in the reaction mixture was varied from 25 to 39 vol% (Table 1). Additionally, two reference experiments were carried out in a single substrate mode, with TCE or AN only. It can be seen that the process is characterized by the presence of a rather prolonged induction period (IP), during which the sample weight increases slowly. For the quantitative comparison of the experiments, the IP duration was taken as a time corresponding to a 500% weight increase (IP-500). As follows from the data presented in Table 1, the IP-500 values vary in a range of 10–20 min. There is also a tendency that an increase in the AN concentration prolongs the induction period. After the IP, the mass of the sample increases linearly in almost all the cases (Fig. 2a). Such a constant rate of carbon deposition indicates that no catalyst deactivation occurs within the time interval of the experiment (2 h).

It should be noted that the addition of acetonitrile vapors to the reaction mixture leads to a noticeable increase of the carbon yield by 80% if compared to the decomposition of pure TCE (Fig. 2a). At the same time, as follows from the carbon yield diagram (Fig. 2b), for the first 30 min of the reaction, the carbon yield values for all the samples are close to each other and amount to approximately 25 g/g(cat). The only exception is the TCE/AN(39)_CNF sample showing the lowest carbon yield. After 1 h of the reaction, the TCE/AN(33)_CNF sample occupied the leading position, while other samples demonstrated comparable values of carbon yield. At the end of the experiments, the samples can be ranked by the carbon yield in the following order: TCE/AN(33)_CNF > TCE/AN(28)_CNF > TCE/AN(25)_CNF > TCE/AN(0)_CNF > > TCE/AN(39)_CNF. The maximum yield of CNF achieved during 2 h for the TCE/AN(33)_CNF sample amounted to 203 g/g(cat). A further increase in the AN concentration leads to a sharp decrease in the weight of carbon deposits. An additional reference experiment was performed with pure AN as a decomposing substrate. In this case, the growth of CNFs is suppressed (Fig. 2a). The carbon yield was estimated to be 0.7 g/g(cat). Despite the fact that acetonitrile molecule contains carbon and nitrogen atoms and can serve as their source for the N-CNFs formation, the initial stages of the MD process are not realized as efficiently as in the case of chlorine-containing reaction mixtures.

It is of special interest to compare the obtained result on the joint decomposition of TCE and AN with recently published data. Thus, catalytic decomposition of 1,2-dichloroethane over the NiMoW alloy of similar composition at 600 °C during 2 h results in the carbon yield not exceeding 50 g/g(cat) [39]. Herein, the corresponding carbon yield values are 2–4 times higher, which can be explained by the presence of C=C bond in the TCE molecule. As known, unsaturated hydrocarbons are more prone to chemisorption on nickel surfaces with subsequent destruction. The addition of the AN vapors to the reaction mixture naturally leads to an increase in the CNF yield since two additional carbon atoms come from the acetonitrile molecule. Another important issue, which can be supposed, is the possible competitive chemisorption of TCE and AN molecules at the same surface sites of the alloy. This can explain the dramatic drop in activity (carbon deposition) when the AN content was increased from 33 to 39 vol%. Most probably, chemisorbed CH₃CN molecules block most sites on the nickel surface from contact with TCE, thus decreasing the efficiency of its decomposition and slowing the MD process.

Characterization of the obtained CNFs

The morphology and secondary structure of the CNFs obtained by the joint catalytic decomposition of TCE and AN were investigated by SEM. Corresponding SEM images are shown in Fig. S2. As seen, the carbon product is mainly represented by long filaments of submicron diameter. Some of them are straight and elongated, while others are chaotically interlaced. The segmented structure of elongated fibers is more evidently seen in Fig. S2b. Such a unique structure is generally inherent in the carbon materials derived from chlorine-substituted hydrocarbons [49, 52, 53]. It is worth noting that the AN concentration in the reaction mixture does not noticeably affect the structure and morphology of the deposited CNFs. This means that exactly chlorine-containing substrate plays a role of a structure-defining reagent.

Electron microscopy data (Fig. S2e) also revealed that in the case of the single-substrate decomposition (pure AN), the morphology of the carbon product sharply differs from the typical filamentous structure. In this case, the MD process of the initial alloy is supposed to be suppressed, and the formation of active particles catalyzing the CNFs growth is significantly decelerated. Therefore, the presence of the chlorine-containing reagent seems to be the necessary condition for the efficient realization of the MD process. In this regard, precise investigation of the early stages of the MD process is of great importance.

While considering the processes taking place during the induction period, the main attention should be paid to the first 10 min. These key processes are the rapid disintegration of the initial alloy in an aggressive reaction medium and the nucleation of the active sites for CNFs growth. Two points of the experiment duration (2 and 5 min) were chosen to study the initial stages in detail. In these cases, the samples of the ternary NiMoW alloy were exposed to contact with the TCE/AN/H₂/Ar reaction mixture containing 25 vol% of AN. The process was stopped after mentioned periods of time by cooling the reactor with an argon flow. The obtained samples were examined by SEM and TEM techniques.

SEM data revealed that within 2 min of exposure, the smooth surface of the initial NiMoW alloy becomes rougher due to the chemisorption of the organic substrates and deposition of carbon (Fig. S3a, b). The appearance of short carbon filaments is already well seen. At this stage, the microdispersed alloy remains its initial ‘sponge-like’ structure. The situation has changed dramatically already after 5 min of exposure. The morphology of the alloy sample undergoes crucial changes, as shown in Fig. S3c. The surface of the alloy became completely covered with the carbon deposits represented by short filaments of various diameters. Some fuzzy impression of the initial alloy structure is still discerned. Thus, a noticeable growth of the nanostructured carbon material begins already at the early stages of the process, when the weight gain of the sample is insignificant. Fig. S3d shows the SEM image of the carbon product obtained after 2 h of exposure. Here, bunches of various carbon filaments are only seen.

TEM technique allows studying these early stages of the MD process more precisely. Fig. 3 demonstrates a set of TEM images for the TCE/AN(25)_CNF samples after exposure to the reaction mixture for 2 and 5 min, and 2 h. As clearly seen from these data, the surface of the alloy is rearranged already within the first 2 min.

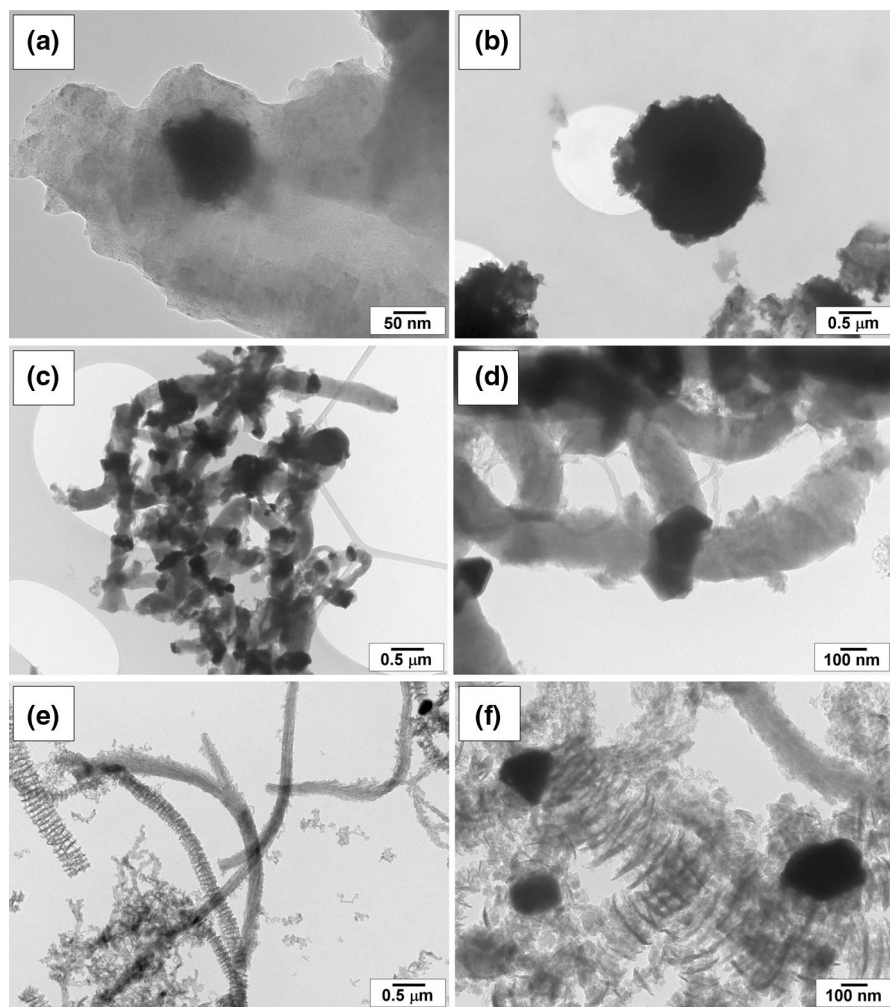


Fig. 3 TEM images of the NiMoW samples exposed to the reaction mixture TCE/AN(25)/H₂/Ar at 600 °C for: 2 min (a, b); 5 min (c, d); 2 h (e, f)

The beginning of the CNFs growth is also evident. Fig. 3b shows small particles of ~100 nm in diameter separated from the bulk of the alloy, thus indicating the destruction of the alloy under the action of the MD process. After 5 min of exposure (Fig. 3c), almost complete disintegration of the NiMoW precursor is observed. The disintegration process is accompanied by the formation of a large number of submicron active particles—former fragments of the initial alloy.

Further, the resulting dispersed metal particles serve as active sites catalyzing the CNFs growth. It is noteworthy that the shape of the crystals separated from the bulk alloy is distinguished by a well-pronounced faceting and angularity (Fig. 3d). Moreover, the size of these newly formed particles exceeds the diameter of the growing

filaments, but, over time, this discrepancy is eliminated. The length of the filaments formed during 5 min of exposure does not exceed 2 μm , while the CNFs diameter varies from 50 to 400 nm, depending on the shape of the active particles. It should be noted that the bi-directional growth of carbon filaments, when two fibers grow in opposite directions on the same active particle, is predominant (Fig. 3d).

Corresponding TEM images of the TCE/AN(25)_CNF samples after 2 h of reaction are presented in Fig. 3e,f. In contrast to the short-time obtained samples, elongated filaments with a distinct stacked or segmented structure are clearly visible (Fig. 3e). Such a secondary structure is explained by an alternation of the chlorination and dechlorination processes on the surface of the metal particles [49, 53]. Besides the segmented nanofibers, the filaments with more uniform packing of graphene layers are also observed (Fig. 3e). However, upon closer examination, the denser structure of CNF is also distinguished by a discrete, ‘mosaic’ structure composed of individual blocks of 20–30 nm in size, as illustrated in Fig. 3f.

Fig. S4 shows the EDX mapping data, demonstrating the distribution of various elements within the structure of the sample. A fragment of the TEM image representing an active metal particle associated with several carbon filaments was selected for analysis. Such elements as C, Ni, Mo, W, Cl, and O were found in the sample. According to the analysis results, the active particle consists of nickel, which is located exclusively within the particle contours. Molybdenum and tungsten are also present in the particle composition. Therefore, the active particle formed as a result of the MD process is a submicron fragment reflecting the composition of the initial alloy. The sample also contains chlorine located mainly on the surface of the metal particle. According to our previously reported observations [49, 54], the complete chlorination of the catalytic particles does not occur under the reaction conditions used in the present study. It was numerously presented that the formation of metal chloride phases completely deactivates the catalyst. Moreover, even after the long-term exposure of the Ni-based alloys to contact with the aggressive chlorine-containing reaction mixture, no nickel chloride reflections are appeared in the XRD patterns [50, 55, 56] thus confirming that the chlorine species are located on the surface. Chlorine atoms remain chemisorbed on the metal surface after the decomposition of the C_2HCl_3 molecules. The coverage of the surface with chlorine species leads to its periodic blocking. Hydrogen present in the composition of the reaction mixture reacts with the chemisorbed chlorine species and, thus, cleans the surface. Such periodic poisoning of the metal surface by chlorine has its consequences. Thus, the second physical stage of the carbide cycle mechanism [33, 45], when carbon atoms diffuse into the bulk of nickel, proceeds impulsively. Finally, this results in the unusual segmented structure of the formed carbon filaments [40]. The appearance of oxygen on the surface of the sample is connected with its adsorption from the atmospheric air during their unloading from the reactor and further storage.

The elemental surface composition of the CNF samples obtained at the varied AN concentration in the reaction mixture was studied using the XPS method. Fig. 4 shows the overview spectra of the synthesized CNF samples with the designation of the lines that make the main contribution to the spectrum. Table 2 summarizes the quantitative data on the concentration of the main elements in the composition of the samples. Analysis of the obtained data confirmed the presence of carbon, nitrogen,

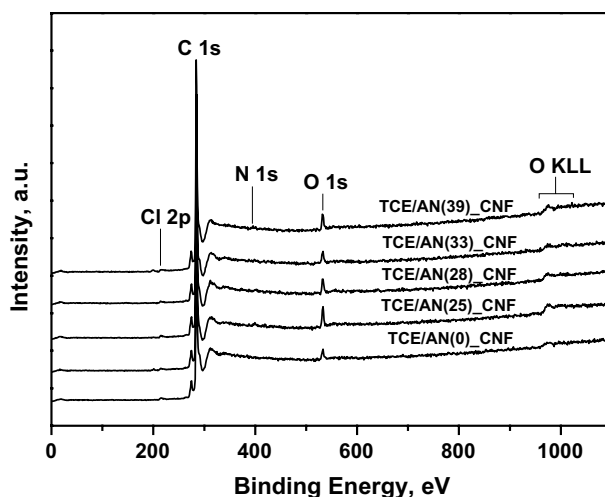


Fig. 4 Survey XPS spectra of the CNF samples obtained using different AN concentrations in the reaction mixture

Table 2 The quantitative surface composition of the CNF samples and the relative concentrations of N, Cl, and O calculated from the XPS data

CNF sample	Content, wt%			Atomic ratio, %		
	N	Cl	O	N_{at}/C_{at}	Cl_{at}/C_{at}	O_{at}/C_{at}
TCE/AN(0)_CNF	–	0.1	3.0	–	0.05	2.3
TCE/AN(25)_CNF	1.3	0.6	6.1	1.2	0.21	5.0
TCE/AN(28)_CNF	0.8	0.3	4.1	0.7	0.10	3.2
TCE/AN(33)_CNF	0.65	0.15	3.8	0.6	0.05	3.0
TCE/AN(39)_CNF	0.5	1.2	5.0	0.5	0.42	4.0

oxygen, and chlorine on the surface of CNFs. The presence of the N 1s line in the spectra demonstrates the principle possibility of obtaining N-functionalized CNFs by the joint decomposition of TCE along with AN over the self-organizing Ni-M catalysts. Oxygen appeared in the composition of the samples after the experiments due to their contact with air is also seen in the spectra.

According to the data presented in Table 2, the maximum nitrogen content of 1.3 wt% is observed for the TCE/AN(25)_CNF sample, which corresponds to the relative concentration $N_{at}/C_{at} = 1.2\%$. It turned out to be interesting that an increase in the acetonitrile concentration in the reaction mixture from 25 to 39 vol% does not result in the expected increase in the number of nitrogen atoms incorporated into the CNFs structure. Oppositely, the N content decreases to 0.5 wt%. It should be emphasized that the revealed tendency is atypical for the two-substrate scheme of the N-CNF synthesis. Usually, the higher concentration of N-containing substrate (for example, NH_3) facilitates an increase in the nitrogen content within the structure of the carbon nanomaterials [57].

The presence of chlorine is also noted in all the samples, which is quite logically explained by the fact that C_2HCl_3 , necessary for the effective course of the MD process, was chosen as one of the reagents. Previously, the presence of chlorine was also registered in the composition of similar carbon materials obtained by decomposition of 1,2-dichloroethane over nickel alloys [40, 58]. In the present study, the maximum amount of chlorine (1.2 wt%) was found in the TCE/AN(39)_CNF sample, which is characterized by the lowest carbon yield value.

Oxygen-containing functional groups are commonly present on the surface of carbon nanomaterials [59]. In our case, the relative oxygen content on the CNF surface (O_{at}/C_{at}) was found to be about 3.5%. The maximum value was observed for the TCE/AN(25)_CNF sample, which possesses the highest nitrogen concentration. According to the low-temperature nitrogen adsorption data, this sample has a significantly higher SSA of 544 m^2/g if compared to all other samples (370–390 m^2/g). The low-temperature nitrogen adsorption/desorption isotherms for the TCE/AN(25)_CNF sample are presented in Fig. S5. According to the IUPAC classification, such isotherms can be assigned to Type II with the ill-defined hysteresis of H3 type that is typical for the open porosity of filamentous carbon materials. Note that IUPAC does not recommend using the conventional methods to calculate the pore size distribution for the qualitative characterization of isotherms of such a type [60]. Therefore, Fig. S6 demonstrates the differential size distribution of the pore volume formally calculated by the regularization technique using a set of root isotherms of nitrogen adsorption at 77.4 K for fissured carbon pores within the QSDFT model [61, 62]. Two character maximums corresponding to the pore width of 1.1 and 3.2 nm are obviously seen. The appearance of these extremums can be connected with the difference in adsorption properties of the studied sample and the reference carbon sample (Cabot BP280) used for the adsorption modeling within the QSDFT model.

Conclusions

The results of the performed research showed that the microdispersed nickel-based alloys could be used as precursors of catalysts for the synthesis of nitrogen-containing carbon nanofibers. The addition of molybdenum and tungsten has previously demonstrated a significant promoting effect on nickel activity in the catalytic decomposition of chlorine-substituted hydrocarbons [39, 40]. The use of a reaction medium containing hydrogen and trichloroethylene leads to a rapid metal dusting of the NiMoW alloy with the formation of submicron particles that serve as active sites for the catalytic CNFs growth. As shown, the simultaneous presence of C_2HCl_3 and CH_3CN vapors in the reaction mixture allows performing the MD process accompanied by the formation (self-organizing) of an active catalyst for the CNFs growth. It was determined that at the optimal ratio of trichloroethylene and acetonitrile concentrations in the reaction mixture, the carbon yield after 2 h of reaction reaches a value of 200 g/g(cat). Such high productivity of Ni catalysts is reported for the first time and exceeds all the experimental data obtained under similar conditions [63]. On the other hand, it should be emphasized that the replacement of trichloroethylene with

acetonitrile (switch to a single-substrate scheme) leads to almost complete suppression of the metal dusting process, thus preventing the formation of an active catalyst.

A detailed study of the surface composition of the obtained CNFs revealed that the joint decomposition of C,Cl- and C,N-containing substrates allows synthesizing carbon materials with a nitrogen content of 0.5 to 1.3 wt%. According to the XPS data, in addition to nitrogen, residual chlorine (up to 1.2 wt%) and oxygen (from 3 to 6 wt%) species are also present on the CNFs surface. If chlorine obviously comes from trichloroethylene, when the appearance of oxygen-containing surface groups is explained by the chemisorption of oxygen from the air.

Thus, a simple and efficient method of one-step synthesis of the N-containing carbon nanofibers using the metal dusting phenomenon as a key tool has been proposed. The produced filamentous carbon nanomaterials possess developed SSA and a unique segmented structure. The appearance of the nitrogen-containing functional groups on the CNFs surface makes this type of material very attractive for subsequent application in sorption and catalysis [64, 65].

Supplementary Information The online version contains supplementary material available at <https://doi.org/10.1007/s11144-022-02169-y>.

Acknowledgements Characterization of the samples was carried out using the equipment of the Center of Collective Use ‘National Center of Catalysts Research’. Authors are grateful to A.N. Serkova for her help in SEM studies. TEM studies were performed in the Krasnoyarsk Regional Center of Research Equipment of the Federal Research Center ‘Krasnoyarsk Science Center SB RAS’.

Funding This work was supported by the Ministry of Science and Higher Education of the Russian Federation (Project numbers AAAA-A21-121011390054-1 (ID: 0239-2021-0010) and 121031700315-2).

Data availability Data available on request from the authors.

Declarations

Conflict of interest The authors declare that they have no conflict of interest.

References

1. George YL (2007) High-temperature corrosion and materials applications. ASM International, Ohio. <https://doi.org/10.31399/asm.tb.htcma.t52080097>
2. Grabke HJ, Schütze M (2007) Metal dusting, carburisation and nitridation. Corrosion by carbon and nitrogen. Woodhead Publ, Sawston
3. Chang JK, Tsai HY, Tsai WT (2008) A metal dusting process for preparing nano-sized carbon materials and the effects of acid post-treatment on their hydrogen storage performance. *Int J Hydrog Energy* 33:6734–6742
4. Romero P, Oro R, Campos M, Torralba JM, Guzman VR (2015) Simultaneous synthesis of vertically aligned carbon nanotubes and amorphous carbon thin films on stainless steel. *Carbon* 82:31–38
5. Taha TJ, Mojet BL, Lefferts L, Meer TH (2016) Effect of carbon nanofiber surface morphology on convective heat transfer from cylindrical surface: synthesis, characterization and heat transfer measurement. *Int J Therm Sci* 105:13–21
6. Nerushev OA, Novopashin SA, Smovzh DV (2008) Synthesis of carbon nanofibers on an austenitic stainless steel. *Nanotechnol Russ* 3:7–8
7. Li LL, Pan LJ, Li DW, Zhao Q, Ma H (2014) Field emission properties of carbon nanocoils synthesized on stainless steel. *New Carbon Mater* 29(1):34–40

8. Tribolet P, Kiwi-Minsker L (2005) Carbon nanofibers grown on metallic filters as novel catalytic materials. *Catal Today* 102–103:15–22. <https://doi.org/10.1016/j.cattod.2005.02.030>
9. Ren G, Pan X, Bayne S, Fan Z (2014) Kiloherz ultrafast electrochemical supercapacitors based on perpendicularly-oriented graphene grown inside of nickel foam. *Carbon* 71:94–101. <https://doi.org/10.1016/j.carbon.2014.01.017>
10. Maubane MS, Bhoware SS, Shaikjee A, Coville NJ (2017) From carbon dots to multipods—The role of nickel particle shape and size. *Diam Relat Mater* 72:53–60. <https://doi.org/10.1016/j.diamond.2016.12.023>
11. Sridhar D, Omanovic S, Meunier JL (2018) Direct growth of carbon nanofiber forest on nickel foam without any external catalyst. *Diam Relat Mater* 81:70–76. <https://doi.org/10.1016/j.diamond.2017.11.011>
12. Ochoa-Fernandez E, Chen D, Yu Z, Totdal B, Ronning M, Holmen A (2005) Carbon nanofiber supported Ni catalyst: effects of nanostructure of supports and catalyst preparation. *Catal Today* 102–103:45–49. <https://doi.org/10.1016/j.cattod.2005.02.005>
13. Ruiz-Cornejo JC, Vivo-Vilches JF, Sebastian D, Martinez-Huerta MV, Lazaro MJ (2021) Carbon nanofiber-supported tantalum oxides as durable catalyst for the oxygen evolution reaction in alkaline media. *Renew Energy* 178:307–317. <https://doi.org/10.1016/j.renene.2021.06.076>
14. Netskina OV, Tayban ES, Moiseenko AP, Komova OV, Mukha SA, Simagina VI (2015) Removal of 1,2-dichlorobenzene from water emulsion using adsorbent-catalysts and its regeneration. *J Hazard Mater* 285:84–93. <https://doi.org/10.1016/j.jhazmat.2014.10.017>
15. Gusain R, Kumar N, Ray SS (2020) Recent advances in carbon nanomaterial-based adsorbents for water purification. *Coord Chem Rev* 405:213111. <https://doi.org/10.1016/j.ccr.2019.213111>
16. Fiorani A, Merino JP, Zanut A, Criado A, Valenti G, Prato M, Paolucci F (2019) Advanced carbon nanomaterials for electrochemiluminescent biosensor applications. *Curr Opin Electrochem* 16:66–74. <https://doi.org/10.1016/j.coelec.2019.04.018>
17. Lebedeva MV, Gribov EN (2020) Electrochemical behavior and structure evolution of polyaniline/carbon composites in ionic liquid electrolyte. *J Solid State Electrochem* 24:739–751. <https://doi.org/10.1007/s10008-020-04516-2>
18. Loh KP, Ho D, Chiu GNC, Leong DT, Pastorin G, Chow EKH (2018) Clinical applications of carbon nanomaterials in diagnostics and therapy. *Adv Mater* 30:1802368. <https://doi.org/10.1002/adma.201802368>
19. Wang S, Lim JLG, Tan KH (2020) Performance of lightweight cementitious composite incorporating carbon nanofibers. *Cement Concr Comp* 109:103561. <https://doi.org/10.1016/j.cemconcomp.2020.103561>
20. Rashad AM (2017) Effect of carbon nanotubes (CNTs) on the properties of traditional cementitious materials. *Constr Build Mater* 153:81–101. <https://doi.org/10.1016/j.conbuildmat.2017.07.089>
21. Wang T, Xu J, Meng B, Peng G (2020) Experimental study on the effect of carbon nanofiber content on the durability of concrete. *Constr Build Mater* 250:118891. <https://doi.org/10.1016/j.conbuildmat.2020.118891>
22. Xin X, Liang M, Yao Z, Su L, Zhang J, Li P, Sun C, Jiang H (2020) Self-sensing behavior and mechanical properties of carbon nanotubes/epoxy resin composite for asphalt pavement strain monitoring. *Constr Build Mater* 257:119404. <https://doi.org/10.1016/j.conbuildmat.2020.119404>
23. Santiago-Calvo M, Tirado-Mediavilla J, Rauhe JC, Jensen LR, Ruiz-Herrero JL, Villafane F, Rodriguez-Perez MA (2018) Evaluation of the thermal conductivity and mechanical properties of water blown polyurethane rigid foams reinforced with carbon nanofibers. *Eur Polym J* 108:98–106. <https://doi.org/10.1016/j.eurpolymj.2018.08.051>
24. Podyacheva OY, Ismagilov ZR (2015) Nitrogen-doped carbon nanomaterials: to the mechanism of growth, electrical conductivity and application in catalysis. *Catal Today* 249:12–22. <https://doi.org/10.1016/j.cattod.2014.10.033>
25. Suboch AN, Podyacheva OY (2021) Pd catalysts supported on bamboo-like nitrogen-doped carbon nanotubes for hydrogen production. *Energies* 14:1501. <https://doi.org/10.3390/en14051501>
26. Ma PC, Siddiqui NA, Marom G, Kim JK (2010) Dispersion and functionalization of carbon nanotubes for polymer-based nanocomposites: a review. *Composites Part A* 41:1345–1367. <https://doi.org/10.1016/j.compositesa.2010.07.003>
27. Pan G, Cao F, Zhang Y, Xia X (2020) N-doped carbon nanofibers arrays as advanced electrodes for supercapacitors. *J Mater Sci Technol* 55:144–151. <https://doi.org/10.1016/j.jmst.2019.10.004>

28. Kumar S, Srivastva AN (2021) Application of carbon nanomaterials decorated electrochemical sensor for analysis of environmental pollutants. IntechOpen Ltd, London. <https://doi.org/10.5772/intechopen.96538>
29. Ruiz-Garcia C, Heras F, Calvo L, Alonso-Morales N, Rodriguez JJ, Gilarranz MA (2020) Improving the activity in hydrodechlorination of Pd/C catalysts by nitrogen doping of activated carbon supports. *J Environ Chem Eng* 8(2):103689. <https://doi.org/10.1016/j.jece.2020.103689>
30. Maboya WK, Coville NJ, Mhlanga SD (2016) The synthesis of carbon nanomaterials using chlorinated hydrocarbons over a Fe-Co/CaCO₃ catalyst. *S Afr J Chem* 69:15–26. <https://doi.org/10.17159/0379-4350/2016/v69a3>
31. Podyacheva OY, Shmakov AN, Boronin AI, Kibis LS, Koscheev SV, Gerasimov EY, Ismagilov ZR (2013) A correlation between structural changes in a Ni-Cu catalyst during decomposition of ethylene/ammonia mixture and properties of nitrogen-doped carbon nanofibers. *J Energy Chem* 22:270–278
32. Mishakov IV, Bauman YI, Shubin YV, Kibis LS, Gerasimov EY, Mel'gunov MS, Stoyanovskii VO, Korenev SV, Vedyagin AA (2020) Synthesis of nitrogen doped segmented carbon nanofibers via metal dusting of Ni-Pd alloy. *Catal Today*. <https://doi.org/10.1016/j.cattod.2020.06.024>
33. Buyanov RA, Chesnokov VV (2006) On mechanism of formation of carbon nanofilaments during catalytic decomposition of hydrocarbons over iron-subgroup metals. *Catal Ind* 2:3–15
34. Nieto-Marquez A, Valverde JL, Keane MA (2009) Selective low temperature synthesis of carbon nanospheres via the catalytic decomposition of trichloroethylene. *Appl Catal A* 352(1–2):159–170. <https://doi.org/10.1016/j.apcata.2008.10.006>
35. Tsai WT (2017) Fate of chloromethanes in the atmospheric environment: implications for human health, ozone formation and depletion, and global warming impacts. *Toxics* 5:23. <https://doi.org/10.3390/toxics5040023>
36. Rudnev AV, Lysakova AS, Plyusnin PE, Bauman YI, Shubin YV, Mishakov IV, Vedyagin AA, Buyanov RA (2014) Ni-Cu and Ni-Co alloys: synthesis, structure, and catalytic activity for the decomposition of chlorinated hydrocarbons. *Inorg Mater* 50(6):613–619. <https://doi.org/10.1134/S0020168514060156>
37. Mishakov IV, Kutaev NV, Bauman YI, Shubin YV, Koskin AP, Serkova AN, Vedyagin AA (2020) Mechanochemical synthesis, structure, and catalytic activity of Ni-Cu, Ni-Fe, and Ni-Mo alloys in the preparation of carbon nanofibers during the decomposition of chlorohydrocarbons. *J Struct Chem* 61(5):811–821. <https://doi.org/10.1134/S0022476620050133>
38. Bauman YI, Mishakov IV, Vedyagin AA, Rudnev AV, Plyusnin PE, Shubin YV, Buyanov RA (2017) Promoting effect of Co, Cu, Cr and Fe on activity of Ni-based alloys in catalytic processing of chlorinated hydrocarbons. *Top Catal* 60(1–2):171–177
39. Shubin YV, Bauman YI, Plyusnin PE, Mishakov IV, Tarasenko MS, Melgunov MS, Stoyanovskii VO, Vedyagin AA (2021) Facile synthesis of triple Ni-Mo-W alloys and their catalytic properties in chemical vapor deposition of chlorinated hydrocarbons. *J Alloys Compd* 866:158778. <https://doi.org/10.1016/j.jallcom.2021.158778>
40. Bauman YI, Rudneva YV, Mishakov IV, Plyusnin PE, Shubin YV, Korneev DV, Buyanov RA (2019) Effect of Mo on the catalytic activity of Ni-based self-organizing catalysts for processing of dichloroethane into segmented carbon nanomaterials. *Heliyon* 5:e02428. <https://doi.org/10.1016/j.heliyon.2019.e02428>
41. Brauer G (1978) *Handbuch der Preparativen Anorganischen Chemie: in drei Banden/Bd 2*, Ferdinand Enke, Stuttgart
42. Nolze G, Kraus W (1998) *Powder Diffr* 13:256–259
43. Krumm S (1996) *Mater Sci Forum* 228–231:183–190. <https://doi.org/10.4028/www.scientific.net/MSF.228-231.183>
44. Cullity BD (1978) *Elements of X-ray diffraction*, 2nd edn. Addison-Wesley, London
45. Mishakov IV, Chesnokov VV, Buyanov RA, Pakhomov NA (2001) Decomposition of chlorinated hydrocarbons on iron-group metals. *Kinet Catal* 42:543–548. <https://doi.org/10.1023/A:1010585808978>
46. Moulder JF, Stickle WF, Sobol PE, Bomben KD (1992) *Handbook of X-ray photoelectron spectroscopy*. Eden Prairie, Minnesota
47. Bauman YI, Kutaev NV, Plyusnin PE, Mishakov IV, Shubin YV, Vedyagin AA, Buyanov RA (2017) Catalytic behavior of bimetallic Ni-Fe systems in the decomposition of 1,2-dichloroethane. Effect of iron doping and preparation route. *Reac Kinet Mech Cat* 121:413–423. <https://doi.org/10.1007/s11144-017-1180-4>

48. Mishakov IV, Bauman YI, Potylitsyna AR, Shubin YV, Plyusnin PE, Stoyanovskii VO, Vedyagin AA (2022) Catalytic properties of bulk $(1-x)_{Ni-x}W$ alloys in the decomposition of 1,2-Dichloroethane with the production of carbon nanomaterials. *Kinet Catal* 63:75–86. <https://doi.org/10.1134/S0023158422010037>
49. Bauman YI, Shorstkaya YV, Mishakov IV, Plyusnin PE, Shubin YV, Korneev DV, Stoyanovskii VO, Vedyagin AA (2017) Catalytic conversion of 1,2-dichloroethane over Ni-Pd system into filamentous carbon material. *Catal Today* 293–294:23–32. <https://doi.org/10.1016/j.cattod.2016.11.020>
50. Bauman YI, Rudneva YV, Mishakov IV, Plyusnin PE, Shubin YV, Vedyagin AA (2018) Synthesis of filamentary carbon material on a self-organizing Ni-Pt catalyst in the course of 1,2-dichloroethane decomposition. *Kinet Catal* 59:363–371. <https://doi.org/10.1134/S0023158418030023>
51. Bauman YI, Mishakov IV, Vedyagin AA, Serkova AN, Gromov AA (2017) Kinetic features of the carbon erosion of a bulk NiCr alloy during the catalytic decomposition of 1,2-dichloroethane. *Kinet Catal* 58:448–454. <https://doi.org/10.1134/S0023158417040036>
52. Nieto-Marquez A, Valverde JL, Keane MA (2007) Catalytic growth of structured carbon from chloro-hydrocarbons. *Appl Catal A* 332:237–246. <https://doi.org/10.1016/j.apcata.2007.08.028>
53. Bauman YI, Lysakova AS, Rudnev AV, Mishakov IV, Shubin YV, Vedyagin AA, Buyanov RA (2014) Synthesis of nanostructured carbon fibers from chlorohydrocarbons over bulk Ni-Cr alloys. *Nanotechnol Russ* 9:380–385
54. Bauman YI, Mishakov IV, Vedyagin AA, Dmitriev SV, MgM S, Buyanov RA (2012) Processing of organochlorine waste components on bulk metal catalysts. *Catal Ind* 4:261–266. <https://doi.org/10.1134/S2070050412040034>
55. Bauman YI, Mishakov IV, Rudneva YV, Plyusnin PE, Shubin YV, Korneev DV, Vedyagin AA (2019) Formation of active sites of carbon nanofibers growth in self-organizing Ni-Pd catalyst during hydrogen-assisted decomposition of 1,2-dichloroethane. *Ind Eng Chem Res* 58(2):685–694. <https://doi.org/10.1021/acs.iecr.8b02186>
56. Mishakov IV, Vedyagin AA, Bauman YI, Potylitsyna AR, Kadtsyna AS, Chesnokov VV, Naliwaiko AY, Gromov AA, Buyanov RA (2020) Two scenarios of dechlorination of the chlorinated hydrocarbons over nickel-alumina catalyst. *Catalysts* 10:1446. <https://doi.org/10.3390/catal10121446>
57. Svintsitskiy DA, Kibis LS, Smirnov DA, Suboch AN, Stonkus OA, Podyacheva OY, Boronin AI, Ismagilov ZR (2018) Spectroscopic study of nitrogen distribution in N-doped carbon nanotubes and nanofibers synthesized by catalytic ethylene-ammonia decomposition. *Appl Surf Sci* 435:1273–1284. <https://doi.org/10.1016/j.apsusc.2017.11.244>
58. Bauman Y, Kibis L, Mishakov I, Rudneva Y, Stoyanovskii V, Vedyagin A (2019) Synthesis and functionalization of filamentous carbon material via decomposition of 1,2-dichloroethane over self-organizing Ni-Mo catalyst. *Mater Sci Forum* 950:180–184. <https://doi.org/10.4028/www.scientific.net/MSF.950.180>
59. Aoki K, Senga R, Suga Y, Totani K, Maki T, Itoh H, Shinokura K, Suenaga K, Watanabe T (2017) Structural analysis and oxygen reduction reaction activity in bamboolike nitrogen-doped carbon nanotubes containing localized nitrogen in nodal regions. *Carbon* 123:99–105. <https://doi.org/10.1016/j.carbon.2017.03.087>
60. Thommes M, Kaneko K, Neimark AV, Olivier JP, Rodriguez-Reinoso F, Rouquerol J, Sing KSW (2015) Physisorption of gases, with special reference to the evaluation of surface area and pore size distribution (IUPAC Technical Report). *Pure Appl Chem* 87:1051–1069. <https://doi.org/10.1515/pac-2014-1117>
61. Neimark AV, Lin Y, Ravikovitch PI, Thommes M (2009) Quenched solid density functional theory and pore size analysis of micro-mesoporous carbons. *Carbon* 47:1617–1628. <https://doi.org/10.1016/j.carbon.2009.01.050>
62. Gor GY, Thommes M, Cychosz KA, Neimark AV (2012) Quenched solid density functional theory method for characterization of mesoporous carbons by nitrogen adsorption. *Carbon* 50:1583–1590. <https://doi.org/10.1016/j.carbon.2011.11.037>
63. Mishakov IV, Vedyagin AA, Bauman YI, Shubin YV, Buyanov RA (2018) Synthesis of carbon nanofibers via catalytic chemical vapor deposition of halogenated hydrocarbons. In: Lee C-S (ed) *Carbon nanofibers: synthesis, applications and performance*. Nova Science Publ, New York
64. Evtushok VY, Podyacheva OY, Suboch AN, Maksimchuk NV, Stonkus OA, Kibis LS, Kholdceva OA (2020) H_2O_2 -based selective oxidations by divanadium-substituted polyoxotungstate

- supported on nitrogen-doped carbon nanomaterials. *Catal Today* 354:196–203. <https://doi.org/10.1016/j.cattod.2019.03.060>
65. Pelech R, Milchert E, Wrobel R (2006) Adsorption dynamics of chlorinated hydrocarbons from multi-component aqueous solution onto activated carbon. *J Hazard Mater* 137:1479–1487. <https://doi.org/10.1016/j.jhazmat.2006.04.023>

Publisher's Note Springer Nature remains neutral with regard to jurisdictional claims in published maps and institutional affiliations.